WAVELET ANALYSIS OF THE TURBULENT JET

R. EVERSON, L. SIROVICH

Center for Fluid Mechanics and the Division of Applied Mathematics, Brown University, Providence, RI 02912, USA

and

K.R. SREENIVASAN

Yale University, Department of Mechanical Engineering, New Haven, CT 06520, USA

The wavelet transform is applied to two-dimensional dye concentration data in turbulent jets at moderate Reynolds numbers. This reveals the nature and limitations of scale similarity of the inner structure of the scalar, and the stringiness associated with small scales. For comparison, two-dimensional Brownian motion is also treated.

The wavelet transform [1–3] has recently been applied to turbulence data [4,5]. It was suggested that the bifurcating patterns which resulted gave visual evidence that the Richardson cascade [6] was present. However, it was shown in another investigation [7] that a process as non-deterministic as Brownian motion produces a visually similar bifurcating pattern to that of atmospheric and other turbulence data [8,9]. Therefore, while the assertion about the cascade may be true, further analysis is clearly indicated. In the present investigation we apply the wavelet transform to the study of two-dimensional axial and meridional sections of a turbulent round jet flow [10]. (This is in contrast to the above cited works, most of which are restricted to one-dimensional records. Exceptions are the work of Argoul et al. [12] and Arneodo et al. [13] in which the wavelet transform is applied to two-dimensional aggregates and the recent treatment of two-dimensional turbulence by Farge and Rabreau [14]. We have also applied wavelet transforms to the three-dimensional jet data of ref. [11], but this will not be presented here.) As we will show, the wavelet transform, which is primarily a visual tool, is well suited to revealing the similarity and inner structure of a flow. It also leads to physical insights which only have

been hinted at in previous discussions of the turbulent jet.

The wavelet transform of a function $u(x)$ is defined as

$$U(a, x) = \frac{1}{a^{N/2}} \int_{-\infty}^{\infty} g\left(\frac{x-y}{a}\right) u(y) \, dy, \qquad (1)$$

where $N = \dim[x]$ is the dimension of the space. $g(x)$ is localized at the origin and satisfies

$$\int g(x) \, dx = 0. \qquad (2)$$

Most previous applications of the transform were to time records and questions of causality led to complex $g(x)$ [15]. In the present instance we consider genuine spatial records and such fine points can be disregarded. Also, while different wavelet functions have been proposed they appear to produce no truly significant variations in the results [4]. In the following we take

$$g(x) = \nabla^2 \exp(-x^2/2)$$
$$= (x^2 - 1) \exp(-x^2/2), \qquad (3)$$

which is known as the *Mexican hat*.

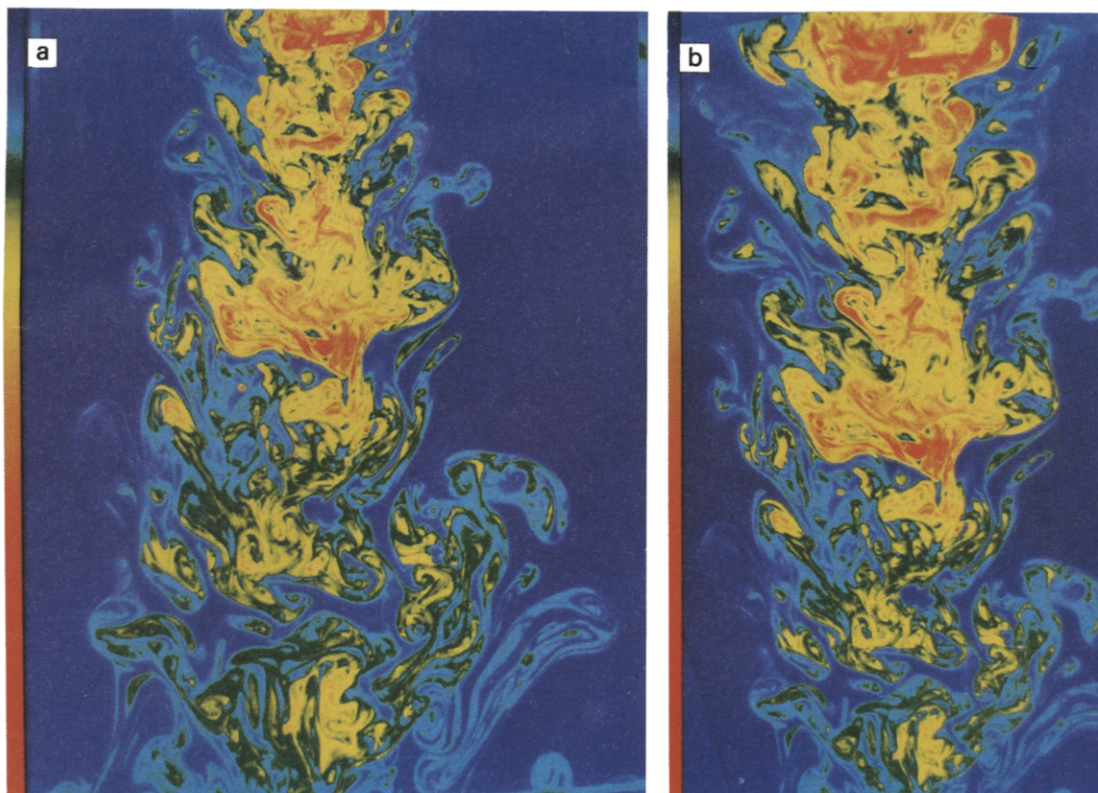In fig. 1a we display a two-dimensional laser in-

Fig. 1. (a) A laser-induced-fluorescence image of a two-dimensional section of a turbulent jet at a nozzle Reynolds number of about 4000. Different colors indicate different levels of concentration, with deep red indicating the largest level and the deep blue indicating the background or zero concentration. The color strip alongside the plate indicates the color code used in the picture. (b) shows the conformally mapped jet as discussed in the text. The streamwise inhomogeneity in concentration has been *adjusted* by the normalization discussed. This is the image on which the wavelet analysis has been presented.

duced fluorescence image of a longitudinal slice of an axisymmetric water jet [9]. The nozzle Reynolds number was 4000, the Schmidt number of the dye particle [16] is of order 1000 (which can therefore be regarded as non-diffusing) and the image covers approximately 8 to 24 nozzle diameters downstream. The image was captured digitally on approximately 1000×1000 pixel files, each pixel having a range of 2^{12} gray levels. The average Kolmogorov scale in the image is approximately 2 pixels. Direct application of the wavelet transform to the image shown in fig. 1a does not reveal the true inner structure of the flow because of the spread of the jet and the consequent streamwise inhomogeneity. This can be corrected to show the structure in a more revealing fashion. The underlying physics of

the turbulent jet provides us with a framework for dealing with this issue, and this is now briefly reviewed.

A schematic of the jet is indicated in fig. 2. Well away from the nozzle we conclude, on dimensional grounds, that the diameter of the jet scales as

$$y \propto x. \tag{4}$$

The same $O(x)$ growth is also true for the Kolmogorov scale. From conservation of momentum transport in the downstream direction the axial velocity scales as [17]

$$U \propto \frac{1}{x}. \tag{5}$$

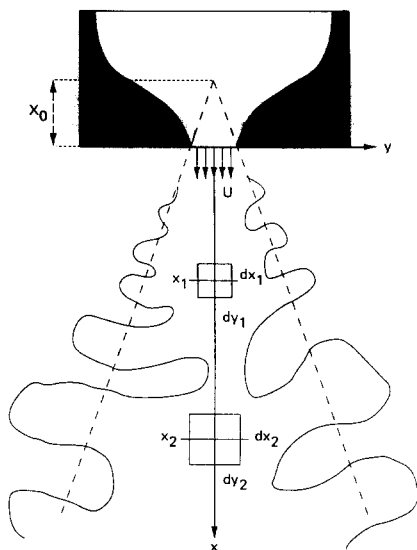As a result, the Reynolds number remains constant.

315

Fig. 2. A schematic of the jet. The linear growth rate of the far field extrapolates to zero at a visual origin x_0 which in this case is about $3\frac{1}{2}$ nozzle diameters upstream of the nozzle. The nozzle contour and upstream flow management is standard. See ref. [11] for details. The basis of conformal mapping, eq. (7), is that the area element $dx_1 dy_1$ centered at x_1 grows linearly to the area element $dx_2 dy_2$ centered at x_2. The interface convolutions are only schematic emphasizing downstream growth of scales, and should not be interpreted literally.

Since the flux of dye concentration is constant, we conclude from the scaling of (4) that the average center line concentration is

$$c \propto \frac{1}{x} . \tag{6}$$

That the concentration is not constant (in spite of the high Schmidt number) is a result of the entrainment of unmarked fluid and its relatively rapid *digestion* by the dyed fluid.

These remarks indicate that there is a similarity, in the statistical sense, in the flow as indicated in fig. 2. Thus the two boxes indicated in the figure scale with distance according to $(dx_1, dy_1):x_1 = (dx_2, dy_2):x_2$. These as well as the previous remarks indicate the image in fig. 1a will be rendered homogeneous in the longitudinal direction (statistically) if we introduce the conformal map

$$Z = \ln(x + iy) . \tag{7}$$

This, as is well known, transforms a wedge to a slot [18]. Equivalently, we transform

$$(x, y) = (r, \theta) = (e^s, \theta) , \tag{8}$$

where θ is the polar angle and r the radius. Viewed in this frame, the flow is statistically homogeneous in the $s = \ln r$ direction and we, henceforth, use the (s, θ) coordinate system. In addition the contrast of the image in fig. 1a should be enhanced linearly as indicated by the falloff in concentration, (6), in order to achieve homogeneity in contrast. The result of these operations on fig. 1a is shown in fig. 1b. The virtual origin of fig. 1a lies roughly 3.5 nozzle diameters upstream of the nozzle. It is clear that in the (s, θ) coordinates this exhibits far more homogeneity in the downstream-direction than does fig. 1a. Fluctuations from the mean behavior exist and therefore the correction for the inhomogeneity is not complete. Comparison of the two plates also indicates the conformal nature of the map, (4). Local shapes remain invariant under the map; for example, circle-like structures go into circle-like structures. The conformally transformed picture also brings out the presence of five or six large scale structures, which is the number of structures predicted by similarity. This is not apparent from fig. 1a, itself.

One further preliminary discussion will be useful before applying the wavelet analysis to the image in fig. 1b. In fig. 3 we show two-dimensional *noise* generated by the Brownian process. Brownian motion in the plane is a random field $U(x)$, $x \in \mathbb{R}^2$, whose increments, $U(x_1) - U(x_2)$, are normally distributed with mean zero and variance given by

$$\langle |U(x_1) - U(x_2)|^2 \rangle \propto |x_1 - x_2| . \tag{9}$$

Details for the procedure for generating this Brownian process are given by Mandelbrot and van Ness [19]. The left column of fig. 4 contains the wavelet transforms of the image shown in fig. 3 under successively smaller scalings, a, indicated in the caption. (Unlike one-dimensional records, where a complete wavelet transform can be rendered as a single image, we now need a series of images, one for each scaling, a, to represent the transform.) These images now serve as characteristic images for the wavelet transform of a non-deterministic phenomenon, and can be compared with the wavelet transform of turbulent flows such as the jet in fig. 1. In
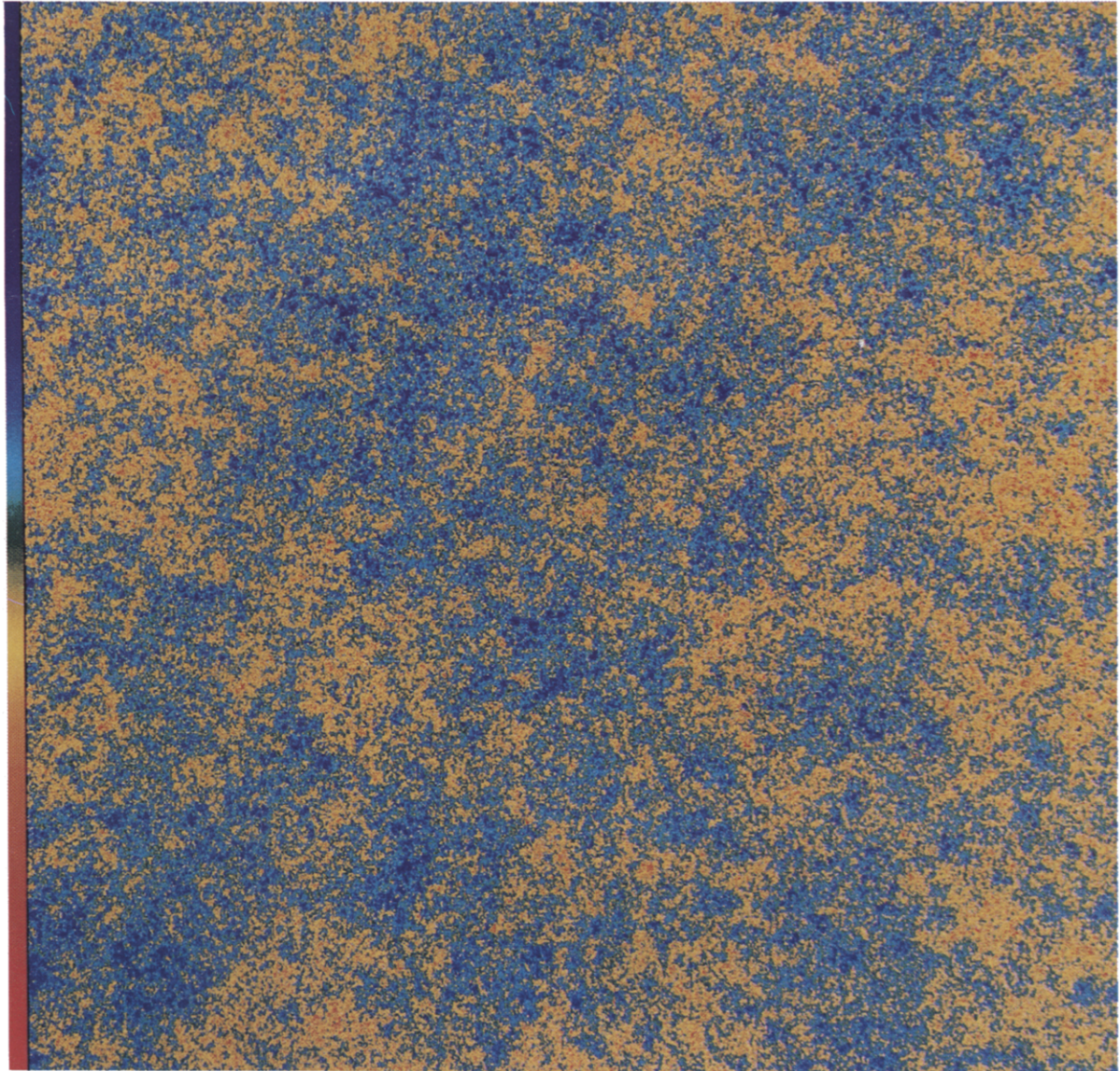
Fig. 3. Brownian motion in the plane generated according to the scheme suggested in ref. [19]. The spatial spectrum falls off like k^{-2}.

addition, it is clear from (9) that Brownian noise should be self-similar or universal under magnification. (For a discussion of self-similarity in one dimension see ref. [20].) In fact [19], as a consequence of (9), we should expect that

$$U(x) \quad \text{and} \quad \frac{1}{a} U(ax) \qquad (10)$$

are statistically indistinguishable.

To explore this idea we show in the right-hand column of fig. 4 the wavelet transforms corresponding to smaller scales, but enlarged to correspond to those on the left. We see that the wavelet transform does bring out the universality. It is the textural identification of these patterns that allows us to conclude that the patterns have the form of (10); i.e. it has
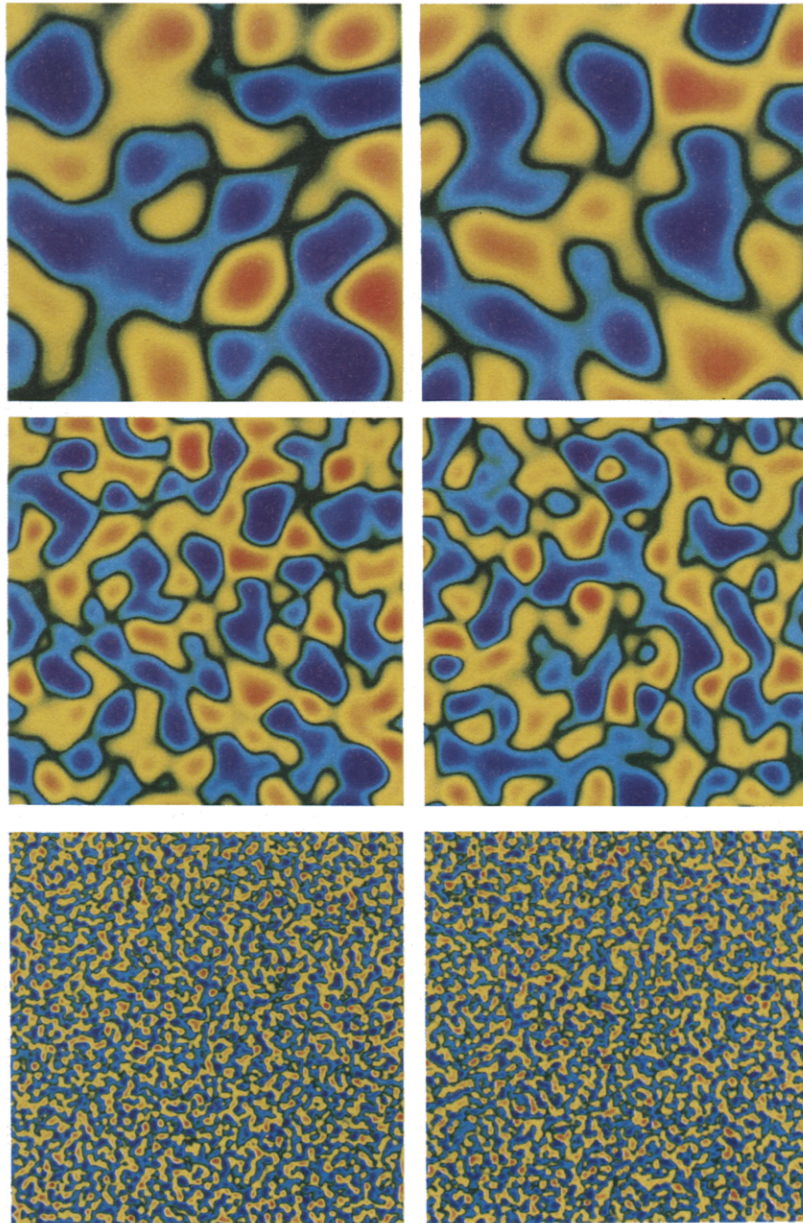
Fig. 4. Wavelet transforms, at scale a of Brownian motion shown in fig. 3. Left-hand column going from top to bottom: $a=0.1$; $a=0.05$; $a=0.01$. Right-hand column, from top to bottom: $a=0.05$, magnified twice; $a=0.02$, magnified two and a half times; $a=0.005$, magnified twice. The linear dimension of each of the pictures in the left column corresponds to $a=1$.

statistically universal form. Moreover, the eye is able to detect this universality. (According to a hypothesis of Julesz [21] the eye classifies texture through

a process that corresponds to forming the autocorrelation.)
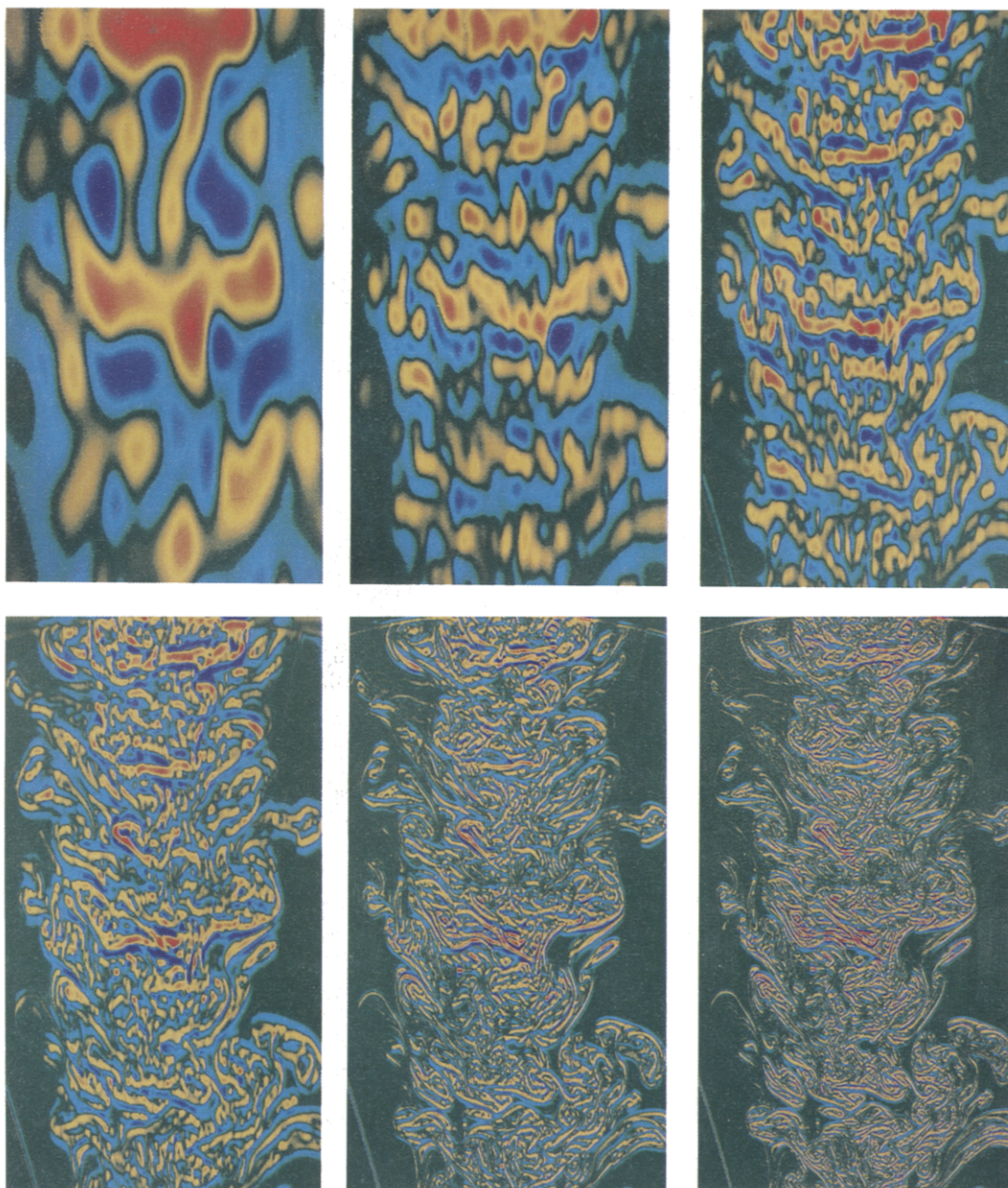
In fig. 5 we show the wavelet transforms of the im-

Fig. 5. Wavelet transforms of the conformally mapped jet shown in fig. 1b. Scale sizes across top row are: $a=0.05$, $a=0.02$, $a=0.01$; across lower row $a=0.005$, $a=0.002$, $a=0.001$. The longer dimension of the picture corresponds to $a=1$.

age in fig. 1b at the indicated scalings, a. The transformed concentration at small scale size decays and therefore each rendition in the sequence of fig. 5 has been normalized so that the highest transformed concentration is displayed as a deep red and the low-est as a deep blue. Green in each signifies the zero point. (A sigmoidal function based on the incomplete beta function is then used to color-code the rest of the picture. See ref. [7] for more details.)
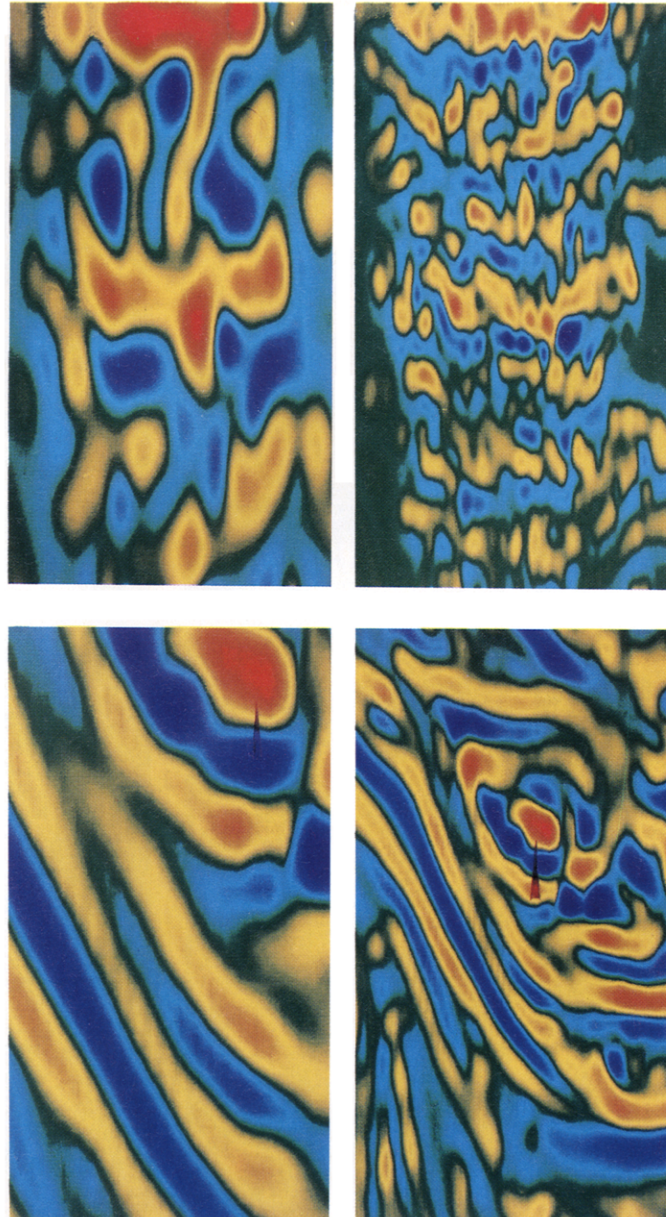
Perhaps the first observation worth making is that

Fig. 6. Upper row contains wavelet transforms of the jet (repeated from fig. 5), going from left to right: $a=0.05$, $a=0.02$, $a=0.01$, $a=0.005$. Second row, going from left to right: $a=0.002$, magnified twenty-five times: $a=0.002$, magnified ten times; $a=0.002$, magnified five times; $a=0.002$, magnified two and a half times. The location of the magnified region is indicated by arrows, which point to the same features in each picture.

there is no resemblance to the Brownian motion images seen in fig. 3. This is in contrast to the similar comparison in the one-dimensional case where a strong resemblance existed between the two [7]. In

fact, we see that there is a great deal of structure at all scalings. Looking from the largest to the smallest scales we see two types of structures present. These we term *beads* and *strings*. Going from $a=0.05$ to
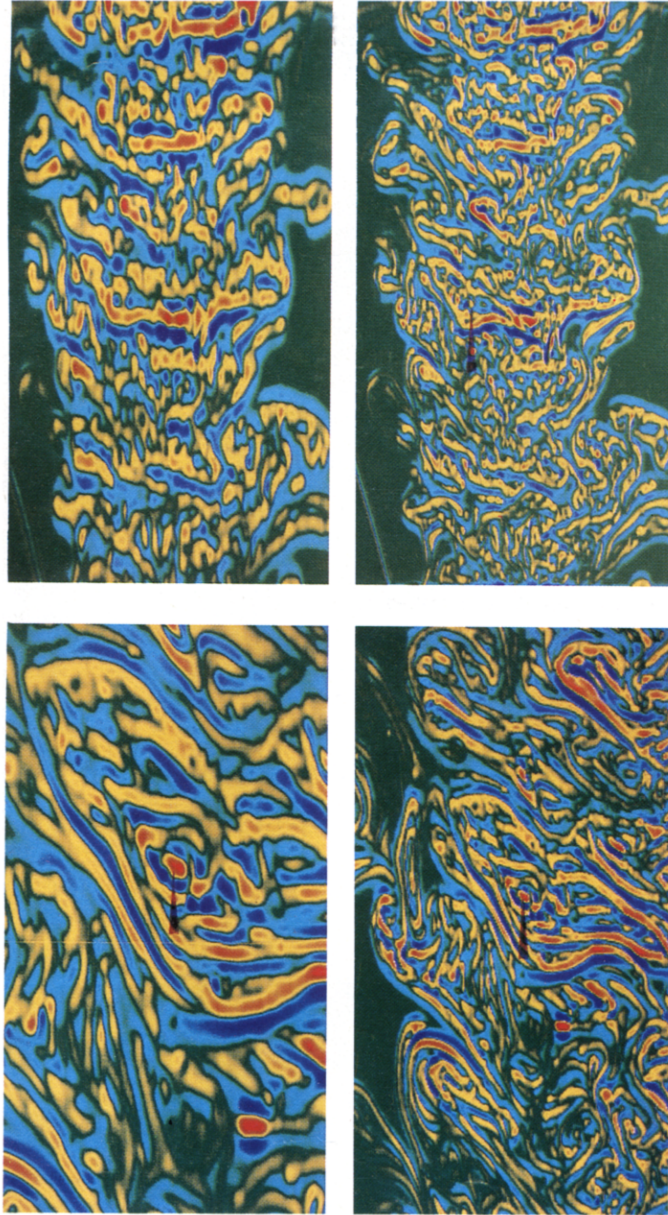
Fig. 6. (Continued).

$a = 0.001$ we see a clear transition from predominantly beads to what appears to be predominantly strings. Two other features are well brought out by the wavelet transform. First, it is clear that the scalar structure is strongly anisotropic. This is perhaps best illustrated by the $a = 0.001$ wavelet transform, which displays the smallest scales of the problem. The same picture also illustrates the transition from the edge region, where the *strings* are aligned at roughly 45° from the axis, to the central region where they are roughly perpendicular to the center line. We note that 45° is the direction of the principal rate of strain of the flow.

The beads are of the extent of the wavelet, viz. *a*. They mark regions of overall concentrations of dye, red, to regions of undyed fluid, blue. The strings are really sheet-like structures as a little thought indicates. Also a wavelet transform of a section meridional to the axis supports this assertion. Such sheet-like structures have already been indicated as spatially high frequency or dissipative structures in the velocity field [22,23]. It is of some importance to observe that sheet-like structures are all very pronounced at $a = 0.001$, when the scale size is in the neightborhood of the Kolmogorov scale. This fact may be of basic importance to our understanding of mixing. Application of wavelets to the three-dimensional data [11] shows that the sheets possess strong three-dimensional convolutions.

Although the wavelet analysis appears to show the transition from *beads* to *strings*, it is necessary to directly investigate the self-similarity of the flow by proceeding, as we did for two-dimensional Brownian motion, through a series of magnifications. This is indicated in fig. 6. The arrows in the bottom four pictures correspond to that in the rightmost picture in the top row. The bottom row contains the magnified versions of the transformed pictures shown in fig. 5. Thus we see that the string-like structures persist under magnification, thus emphasizing the essential lack of self-similarity of the pictures. This is especially true when we focus on the off-axis regions of the jet.

A complete discussion of self-similarity of the inner structure of the jet is hampered by two factors: the moderate jet Reynolds number and the inherent inhomogeneity of the flow. Although we have attempted to correct for this latter aspect in the streamwise direction, it is clearly not complete; no corrections were applied to inhomogeneities in the radial direction.

References

[1] A. Grossmann and J. Morlet, Decomposition of functions into wavelets of constant shape, and related transforms, in: Mathematics and physics; lectures on recent results, ed. L. Streit (World Scientific, Singapore, 1984).

[2] J.M. Combes, A. Grossmann and Ph. Tchamitchian, eds., Wavelets (Springer, Berlin, 1989).

[3] R. Kronland-Martinet, J. Morlet and A. Grossman, Analysis of sound pattern through wavelet transform, Int. J. Patt. Recogn. Art. Intell., special issue on expert systems and pattern analysis (1987).

[4] J. Liandrat and F. Moret-Bailly, Thge wavelet transform: some applications to fluid mechanics and turbulence, Europ. J. Mech. (Fluids) (1988), submitted.

[5] F. Argoul, A. Arnéodo, G. Grasseau, Y. Cagne, E.J. Hopfinger and U. Frish, Nature 338 (1989) 51.

[6] L.F. Richardson, Weather prediction by numerical process (Cambridge Univ. Press, Cambridge, 1922).

[7] R. Everson and L. Sirovich, A survey of wavelet analysis applied to turbulence data, Center for Fluid Mechanics, Brown University, Report 89-182 (1989).

[8] C. Meneveau and K.R. Sreenivasan, in: The physics of chaos and systems far from equilibrium, ed. Minh-Doung Van (North-Holland, Amsterdam, 1987) p. 49.

[9] C. Meneveau and K.R. Sreenivasan, Phys. Rev. Lett. 59 (1987) 1424.

[10] R.R. Prasad, C. Meneveau and K.R. Sreenivasan, Phys. Rev. Lett. 61 (1988) 74.

[11] R.R. Prasad and K.R. Sreenivasan, J. Fluid Mech. (1989), to be published.

[12] F. Argoul, A. Arneodo, J. Elezgaray, G. Grasseau and R. Murenzi, Phys. Lett. A 135 (1989) 327.

[13] A. Arneodo, F. Argoul, J. Elezgaray and G. Grasseau, Wavelet analysis of fractals; application to nonequilibrium phase transitions, in: Nonlinear dynamics, ed. G. Turchetti (World Scientific, Singapore, 1989).

[14] M. Farge and G.C. Rabreau, C.R. Acad. Sci. 307 II (1988) 1479.

[15] A. Grossmann and J. Morlet, SIAM J. Math. Anal. 15 (1984) 723.

[16] B.R. Ware, in: Measurement of suspended particles by quasielastic light scattering, ed. B.E. Dahneke (Wiley, New York, 1983) p. 255.

[17] H. Tennekes and J.L. Lumley, A first course in turbulence (MIT Press, Cambridge, 1972).

[18] L.M. Milne-Thomson, Theoretical hydrodynamics (MacMillan, London, 1949).

[19] B.B. Mandelbrot and J.W. van Ness, SIAM Rev. 10 (1968) 422.

[20] A. Arneodo, G. Grasseau and H. Holschneider, Phys. Rev. Lett. 61 (1988) 2281.

[21] B. Julesz, Nature 290 (1981) 91.

[22] A.Y.S. Kuo and S. Corrsin, J. Fluid Mech. 56 (1972) 447.

[23] K.R. Sreenivasan and C. Meneveau, Phys. Rev. A 38 (1988) 6287.